Frontiers of Physics
https://doi.org/10.1007/s11467-021-1115-4
Front. Phys.
17(2), 23501 (2022)

RESEARCH ARTICLE

Theoretical study of K_3Sb/graphene heterostructure for electrochemical nitrogen reduction reaction

Tianyi Wang[1,2], Ani Dong[3], Xiaoli Zhang[4], Rosalie K. Hocking[2], Chenghua Sun[1,2,†]

[1] *School of Chemical Engineering and Energy Technology, Dongguan University of Technology, Dongguan 523808, China*
[2] *Department of Chemistry and Biotechnology and Centre for Translational Atomaterials, School of Science, Swinburne University of Technology, Hawthorn, VIC 3122, Australia*
[3] *Department of Computer and Information Science, City College of Dongguan University of Technology, Dongguan 523419, China*
[4] *School of Material Science and Engineering, Zhengzhou University, Zhengzhou 450001, China*
Corresponding author. E-mail: [†] *chenghuasun@swin.edu.au*
Received April 30, 2021; accepted September 10, 2021

Instead of the energy-intensive Haber–Bosch process, electrochemical nitrogen reduction reaction (NRR) is an exciting new carbon neutral technique for ammonia synthesis under ambient conditions. In this work, we investigated K-based electrocatalysts theoretically and demonstrated that K_3Sb/graphene performs excellent activity and inhibits hydrogen evolution on alternating reaction pathway. The first hydrogenation step from N_2* to NNH* was found to be the most energetic and limiting step (0.61 eV). Graphene substrate plays the critical role to promote electronic conductivity between K_3Sb and dinitrogen.

Keywords K_3Sb/graphene, $K_{12}Sb_2Se_3$, K_3Sb, nitrogen reduction reaction, DFT calculation

1 Introduction

Ammonia (NH_3) is an indispensable feedstock for agriculture and the chemical industry, and it is also considered as a renewable energy carrier with high hydrogen content. Nowadays, large-scale NH_3 production relies on the Haber–Bosch process under harsh reaction conditions (350–500 °C, 150–300 atm), which is energy-intensive and emission-intensive when H_2 is produced by steam reforming. Electrochemical nitrogen reduction reaction (NRR) is considered a promising alternative of NH_3 synthesis under ambient conditions, which is carbon-free and energy-saving [1–3].

Exploring high selectivity and activity electrocatalysts is crucial for NRR. Tremendous efforts have focused on transition metal (TM) based catalysts, such as Fe, Mo, and Cu, whose *d*-orbital electrons are employed to react with N_2, experiencing electron donation and back donation at the early and late stages of the reactions respectively [4, 5]. While a typical issue is that TM-based electrocataltysts tend to exhibit worse-balance between N_2 cleavage (early stage) and NH_3 dissociation (late stage) [6, 7]. In addition, *d*-orbital electrons of TMs are more likely to form TM–H bond and promote hydrogen evolution reaction (HER) competitor, reducing Faradaic efficiency significantly [8–11]. Recently, main-group catalysts have demonstrated good catalytic performance for NRR, such as cyano group/g-C_3N_4 and $BaCeO_{3-x}N_yH_z$ [12, 13]. The stronger interactions between main-group elements and N_2 absorbers boost the interfacial kinetics together with HER suppression [14, 15]. Particularly, semiconducting compounds containing alkali metals, characterized by higher quantum efficiency and lower cost, overcome the instability of alkali and alkaline metals in NH_3 synthesis [16, 17]. Earth-abundant potassium (K) is a widely employed promoter for the Haber–Bosch process in ammonia industry with high reduction capacity and excellent ion conductivity. Metallic K is a sufficiently strong chemical reductant that cannot be applied aqueous reactions due to strong reactivity with water [18–22]. However, it is useful to explore the possibility of using K as a promotor in NRR catalysts.

The two-dimensional materials (2D) materials become popular candidates for reaction substrates, because of huge surface, special structure and unique physicochemical properties, such as borophene, TCNQ, and MoPc [23–25]. Interfacial engineering is a powerful technique to expedite electronic transportation and reaction kinetics via interfacial coupling between two active components. Due to the larger counterparts contact area and low aggrega-

* Special Topic: Heterojunction and Its Applications (Ed. Chenghua Sun).
This article can also be found at http://journal.hep.com.cn/fop/EN/10.1007/s11467-021-021-1115-4.

tion, 2D/2D heterojunction, especially carbon based catalysts, enhances physicochemical properties and provide more electron transition channels remarkably, and have been employed widely for electrochemical studies [26–32]. It is noteworthy that cost-effective graphene is one the most popular carbon-based supports, and it has a tolerance of acidic or alkaline reaction conditions and a larger surface and ultrafast electronic mobility. In this work, we propose to use graphene hybrid with K-rich 2D materials ($K_{12}Sb_2Se_3$ and K_3Sb) to build heterojunction, based on which full NRR studies have been investigated. Our aim is to explore K-based catalysts for NRR, expecting to break the key limits raised by transition metals. These compounds are selected based on three considerations: (i) both have been synthesized experimentally; (ii) they offer excellent conductivity as need for electrochemical NRR; and (iii) excellent stability, conductivity and reactivity have been demonstrated in batteries and photocatalysis applications [33–38]. For comparison, elementary steps of NRR process on $K_{12}Sb_2Se_3$, K_3Sb and K_3Sb/graphene are evaluated via density functional theory (DFT) calculations. As demonstrated below, both K-site and graphene substrate play key roles in N_2 fixation and reduction, improving the overall NRR feasibility.

2 Computional methods

All optimized geometry and free energy of intermediates were calculated based on the First Functional Theory through the Vienna Ab initio Simulation Package (VASP) [39]. Revised Perdew–Burke–Ernzerhof (RPBE) functional of the generalized gradient approximation (GGA) was used to describe the electron exchange-correlation interactions [40]. The electron-core interactions were examined by the projected augmented wave. The convergences were 0.001 eV·Å^{-1} in force and 10^{-4} eV in energy with 450 eV kinetic energy cutoff. Models were 2 × 2 supercell with 15 Å vacuum space. The K_3Sb/graphene heterostructure was created by using 5 × 4 × 1 and 2 × 2 × 1 supercell of graphene and K_3Sb (50 carbons, 4 antimony and 12 potassium atoms), and the mismatch along the interface of K_3Sb/graphene is about 2.51%. The Monkhorst–Pack k-point sampling of 3 × 3 × 1 [41], and Van der Waals (VdW) interaction was corrected via DFT-D3 method. The Gibbs free energy changes (ΔG) were calculated as followed: $G = E + \Delta E_{ZPE} - T\Delta S$, where E was binding energy difference and ΔE_{ZPE} was zero-point energy difference for hydrogenation steps, as described in our early studies [13, 42]. $T\Delta S$ was term from the Computational Chemistry Comparison and Benchmark database (http://cccbdb.nis.gov/). The Crystal Orbital Hamilton Population (COHP) was calculated via the LOBSTER program in VASP [43]. The VASPsol was employed to investigate reaction intermediates under solvation effect [44]. In addition, transition states were calculated by climbing-image nudged elastic band (CI-NEB) method. Moreover, the thermodynamic stability of K_3Sb/graphene was examined by ab initio molecular dynamic (AIMD) simulation at 300 K (time period: 2 ps, time step: 2 fs).

3 Results and discussion

Figure 1 shows optimized geometries of $K_{12}Sb_2Se_3$, K_3Sb and K_3Sb/graphene, where $K_{12}Sb_2Se_3$ and K_3Sb/graphene are labelled as K/SbSe and K_3Sb/G, respectively. The optimized interlayer distance between K_3Sb and graphene is 3.34 Å.

Generally, electrochemical NRR has been divided into dissociative and associative reaction mechanisms, depending on N_2 adsorption states [45]. For the former, N≡N triple bond is broken to generate N atoms before hydrogenation, while the cleavage of N≡N is end-on configuration under associative mechanism. Specifically, full associative NRR can be achieved through alternating and distal pathways, and dissociative NRR is preformed via enzymatic pathway. On the alternating and enzymatic pathways, two N atoms are hydrogenated with H* alternatively, and then release two NH_3. Otherwise, H atoms attack the distal N atom continuously in the distal pathway. After the release of the first NH_3, protons begin to bind with the other N atom until the second NH_3 formation. Following these paths, potential intermediate states have been fully optimized and presented in Fig. S1.

On the alternating pathway [see Fig. 2(a)], N_2 adsorptions on K/SbSe, K_3Sb and K_3Sb/G are endothermic process with ΔG of 0.41 eV, 0.35 eV and 0.32 eV, respectively. Subsequently, the first hydrogenation of N_2* is an uphill step with ΔG being 2.21 eV and 1.84 eV on K/SbSe and K_3Sb, respectively, which is also the potential-determining step (PDS). For K/SbSe, after the second H* is coupled with NNH* (ΔG = 0.31 eV), the reduction of NHNH* to $NHNH_2$* needs extra energy of 0.17 eV. The ΔG of subsequent hydrogenation reactions are negative, which are −0.89 eV, −0.29 eV and −1.72 eV,

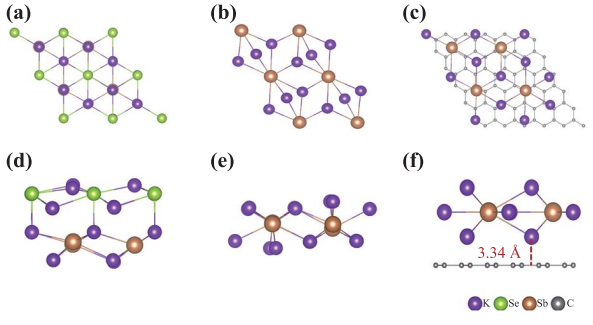

Fig. 1 Optimized geometries of catalysts. **(a–c)** and **(d–f)** are top view and side view of optimized $K_{12}Sb_2Se_3$, K_3Sb and K_3Sb/graphene, respectively.

suggesting the spontaneous nature. In the K_3Sb case, the second H-adding to the other N atom is spontaneous with $\Delta G = -0.09$ eV. After that, the NHNH* is reduced to $NHNH_2$* with small energy demand of 0.05 eV, and then the next hydrogenation step becomes spontaneous again ($\Delta G = -0.48$ eV), releasing the first NH_3 ($\Delta G = -1.37$ eV). Finally, the sixth H* attacks the reaming N with large energy reduce by −0.72 eV. Overall, the initial N_2 reduction is the most challenging step, due to poor activation as described in Fig. 3. Compared with K/SbSe and K_3Sb, graphene substrate can remarkably change the first protonation step, reducing ΔG from 1.84 eV to 0.61 eV, which is still PDS, but performs better than most transitional metals (typically > 1.0 eV). The following hydrogenation reactions are downhill in Gibbs free energy diagram of K_3Sb/G with ΔG are −0.02 eV, −0.01 eV, −0.86 eV and −0.90 eV, correspondingly, until the last protonation step ($\Delta G = 0.44$ eV, for NH_3 release).

On the distal pathway [see Fig. 2(b)], N_2 adsorption and the first hydrogenation have the same ΔG as that of alternating pathway for K/SbSe, K_3Sb and K_3Sb/G. The first H* addition is still the PDS in all cases. The second H* addition on the distal N atom is an uphill step with values of 0.41 eV, 0.62 eV and 0.61 eV for K/SbSe, K_3Sb and K_3Sb/G, respectively, suggesting that N_2 activation faces higher thermodynamic barrier than that on alternating pathway. However, the following hydrogenation reactions on K/SbSe are downhill in energy by −0.74 eV, −0.99 eV, −0.76 eV and −1.08 eV. For K_3Sb, the corresponding ΔG are −1.23 eV, 0.66 eV, −1.94 eV and −0.72 eV. After the first NH_3 releases spontaneously ($\Delta G = -1.74$ eV) on K_3Sb/G, the next protonation step is difficult, labelled by $\Delta G = 0.80$ eV, while the following hydrogenation is spontaneous, until the release of the second NH_3 with energy input ($\Delta G = 0.44$ eV). Overall, K_3Sb/G is the best among the three, favouring the alternating pathway whose first hydrogenation as the PDS with maximum free energy change ($\Delta G_{max} = 0.61$ eV).

In contrast, the N_2 cleavage needs large energy inputs on the enzymatic pathway [Fig. 2(c)]. The ΔG of N_2 dissociation are 0.50, 0.38 and 1.66 eV on K/SbSe, K_3Sb and K_3Sb/G, respectively, inducting that dissociative mechanism is rarely favourable in electrochemical NH_3 synthesis. Besides, the K/SbSe and K_3Sb/G can inhibit HER significantly with more positive ΔG(H*) values than $\Delta G(N_2$*), as shown in Fig. 5(c).

To further understand K–N_2* interaction, charge difference has also been collected and shown in Fig. 3. In the case of K/SbSe, N_2 is adsorbed at single K site with K–N_2 distance of 3.12 Å together with ΔG of 0.41 eV. It is also worth to note that there is nearly no N–N bond elongation (1.119 Å vs 1.115 Å in free N_2 molecular), featured with only 0.01 electrons injected into N–N bond [see Figs. 3(a) and (d)]. Based on all these analysis, it is clear that K/SbSe can hardly activate N_2. Given metallic K is highly active, the above poor performance offered by K/SbSe indicates that fully oxidized K cannot be used as an NRR promoter.

Now we turn to K_3Sb, over which N_2 favours the adsorption over two neighbouring K sites, as shown in Fig. 3(b), with $\Delta G = 0.35$ eV. Interestingly, N–N distance has been slightly enlarged to 1.13 Å, accompanied with an electron transfer of 0.18 e from K_3Sb to N_2, as shown in Fig. 3(e). In other words, K_3Sb may offer NRR catalysis because N_2 has been partially activated under such adsorption. When K_3Sb is loaded on graphene, ΔG for N_2 fixation can be further reduced to 0.32 eV; more impressively, N–N bond length is increased to 1.210 Å and electron transfer up to 0.40 e [see Figs. 3(c) and (f)]. It is obvious that K_3Sb/G is more active with respect to original K_3Sb.

Based on early studies, the binding strength between active sites and N_2 directly affects the following elementary steps and the overall kinetics of full NRR process,

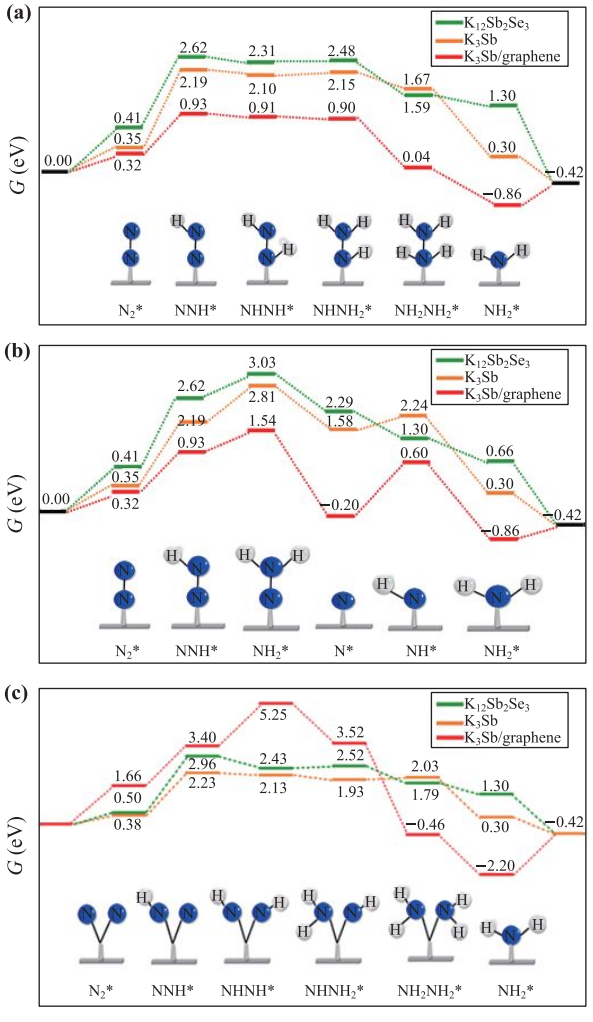

Fig. 2 DFT calculated energy profiles of NRR reaction sequences. Gibbs free energy profiles of **(a)** alternating, **(b)** distal and **(c)** enzymatic reaction pathways on K/SbSe, K_3Sb and K_3Sb/G, respectively.

where too strong N_2 adsorption hinders NH_3 release and vice-verse [46–48]. For these K-based catalysts, N_2 activation and initial hydrogenation are the most difficult steps as identified by energy profile, indicating that K–N_2 interaction needs to be strengthened. This is not surprising because K in these compounds has been oxidized; as a result, its capacity to adsorb and react with N_2 is low, essentially different from K metals.

To gain deep insights into N_2 activation over K-based compounds, the PDOS and –COHP of optimized end-on N_2* intermediations have been calculated, as shown in Fig. 4. For free N_2, the highest occupied molecular orbital (HOMO) and the lowest unoccupied molecular orbital (LUMO) are dominated by 3σ and 2π*, respectively. Herein, the large HOMO–LUMO gap in Fig. 4(a) is consistent with previous calculations, and such gap limits the direct activation through electronic excitation [2, 39, 49]. In the case of K/SbSe, HOMO–LUMO gap for N_2 has almost unchanged, and there is nearly no antibonding state under Fermi level as shown in Fig. 4(b), suggesting that N_2–K interaction is very weak and N_2 still keeps its inert nature. In K_3Sb case, however, N_2 is adsorbed over two K-sites (labelled as K6 and K11), under which occupied orbitals of these K-sites can transfer electrons into N_2 2π* [0.18 e, see Fig. 3(e)]. As a result, a few antibonding states appear at the Fermi level (because N_2 bonding states have been fully occupied) in Fig. 4(c), indicating that N_2 has been partially activated. Such activation becomes more significant in the K_3Sb/G case, in which N_2 is similarly fixed by two K-sites (labelled as K56 and K61). As shown in Fig. 4(d), comprehensive orbital hybridizations between K and N_2 are achieved, together with more charge transfer [0.40 e, see Fig. 3(f)]. This enforces more antibonding states below Fermi level and heavier N_2 activation; as a result, higher reactivity and better performance demonstrated in Fig. 3 can be well understood.

The evolution of –COHP for PDS formation (N_2* + H* → NNH*) on K_3Sb/G was shown in Fig. S2, along with structures of initial state, transition state and final state. In the initial state [see Fig. S2(a)], both bonding and anti-bonding states of N–H are below Fermi level, which are filled with electrons. Such repulsive interaction is the source of hydrogenation barrier, and N–H bond length is 2.30 Å. The anti-bonding moves beyond Fermi level with broaden peak in Fig. S2(b), indicating that anti-bonding of transition state donates electrons with N–H bond length of 1.61 Å. As shown in Fig. S2(c), the anti-bonding of the final state becomes empty, while the energy of bonding states decreases to −12.5 eV with sharp peak and N–H bond length reduces to 1.08 Å, resulting lower system energy.

Given graphene is well known for its large π-bonding, K_3Sb/G junction enables 1.00 e electron transfer from K to graphene [see Figs. 5(a) and (b)]. As electrons donator, K preforms stronger metallicity and interlayer distance increases to 3.73 Å, revealing that the mediation

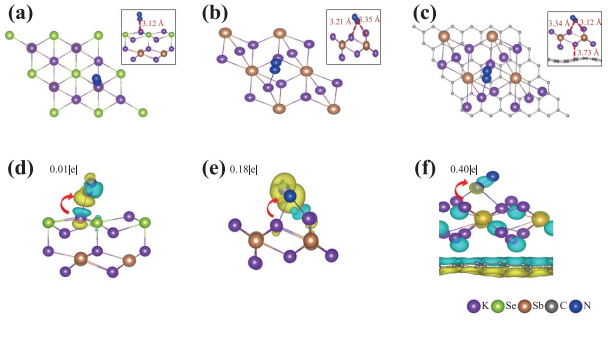

Fig. 3 Optimized geometry and Bader charge difference of N_2* intermediate. **(a–c)** are top view and side view of end-on N_2* intermediates, and **(d–f)** are Bader charge difference on K/SbSe, K_3Sb and K_3Sb/G, respectively.

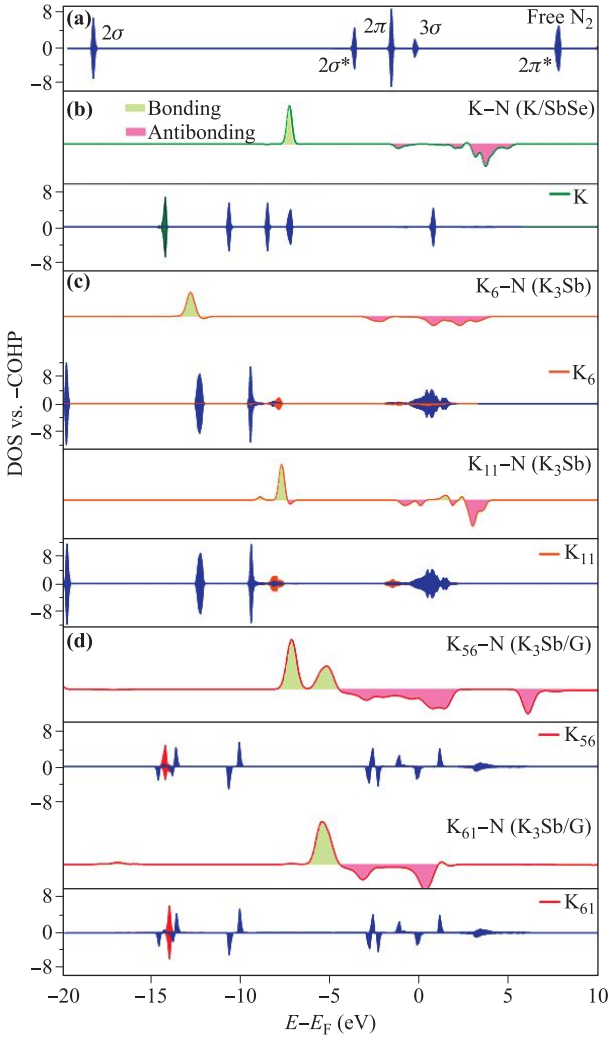

Fig. 4 Chemisorption interaction analysis of end-on N_2* intermediates. **(a)** Molecular orbitals of free N_2. **(b–d)** negative Crystal Orbital Hamilton Populations (–COHPs) and computed partial density of states (PDOS) between K and N of end — on N_2* intermediates on K/SbSe, K_3Sb and K_3Sb/G, respectively. Electrons/eV is the unit of PDOS.

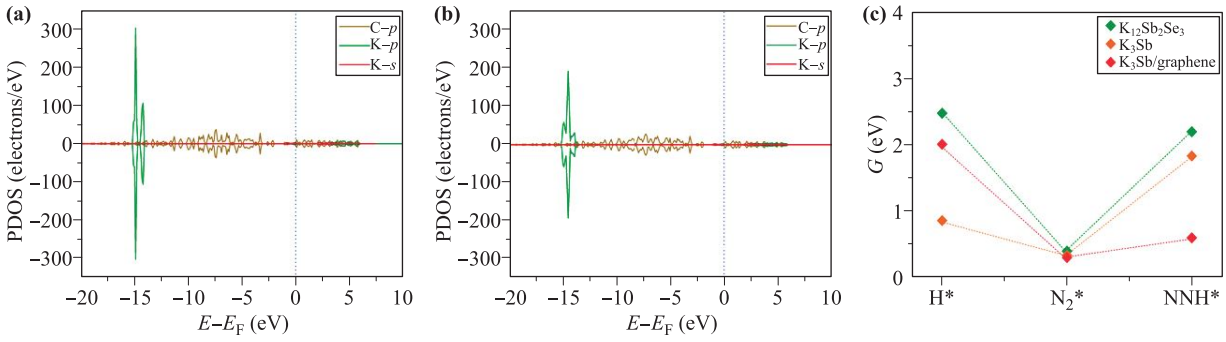

Fig. 5 Chemisorption interaction analysis of K_3Sb/graphene. **(a)** and **(b)** are partial density of states (PDOS) between K and graphene of clean K_3Sb/graphene and N_2* intermediate n K_3Sb/graphene, respectively. **(c)** shows adsorption energies of single H* atom, N_2* and NNH* intermediates on $K_{12}Sb_2Se_3$, K_3Sb and K_3Sb/graphene, respectively.

by graphene substrate plays the key role to promote the catalysis performance of K_3Sb.

Considering aqueous electrolytes in NRR experiments, solvation effect is included on K_3Sb/graphene, and Fig. S3(b) presents the catalytic performance on alternating pathway with and without solvation effect. Under solvation effect, N_2* + H* → NNH* is still the PDS, and $\Delta G = 0.62$ eV is nearly unchanged as compared with that without solvation effect ($\Delta G = 0.61$ eV). Clearly, solvation effect cannot affect K_3Sb/G catalytic activity significantly.

Furthermore, the strain effect is able to alter electronic structure of electrocatalysts, and then influence the reaction intermediates [49, 50]. As shown in Fig. S4(a), the free energy of K_3Sb/G shows linear variation with lattice constants under biaxial stress from −5% to 5%. Similarly, the C–C bond length of graphene elongated with the increase of tensile stress [see Fig. S4(b)]. However, the interlayer distance between K_3Sb and graphene is minimum under no strain effect. Additionally, the catalytic activity is sensitive to strain in horizontal direction. Our results in Fig. S3(a) prove that compressive/tensile stress has negative influence on catalytic activity, suggesting interface between K_3Sb and graphene is sensitive to strain effect. Moreover, as shown in Fig. S5, the AIMD result proposed that the small energy and temperature oscillate and stable structure of K_3Sb/G without significant deformations at 300 K, indicating that the K_3Sb/G has high thermodynamic stability.

It is worth pointing out that N_2 activation by K-species has been experimentally studied recently [13, 51–53], in which K has been introduced as ions from the solution but loaded to porous materials as active site to fix N_2. Its mechanism is similar with this work, but the loading ratio is remarkably different, because herein K, as a major component of the catalyst, is abundant. Given N_2 activation is the first step for full NRR, such inherent active sites do not undermine catalyst stability, making it different from the reactivity brought by vacancies [54–56] or single-atom catalysts [57–61]. Therefore, the activity of K-site can be improved after being loaded on graphene, indicating that the substrate can regulate electronic states of the catalyst and the performance. Such promotion effect associated with catalyst-substrate interactions has been widely reported [62–65], leaving a large space for further optimization of K-based catalysts.

4 Conclusion

Through DFT calculations, we explored the catalysis performance of K-based main group compounds ($K_{12}Sb_2Se_3$ and K_3Sb) for NRR. With respect to $K_{12}Sb_2Se_3$, K_3Sb is more active and its activity can be further improved through the formation of K_3Sb/graphene heterojunction, which offers excellent catalytic performance for NRR process as featured by small thermodynamic barrier ($\Delta G = 0.61$ eV). These findings provide a new insight that alkali-contained semiconducting compounds hybrid with graphene support may be a new option for the design of NRR catalysts.

Electronic supplementary material is available in the online version of this article at https://doi.org/10.1007/s11467-021-1115-4 and is accessible for authorized users.

Acknowledgements The authors acknowledge the financial support by Guangdong Innovation Research Team for Higher Education (No. 2017KCXTD030), High-level Talents Project of Dongguan University of Technology (No. KCYKYQD2017017), Research Center of New Energy Materials (No. KCYCXPT2017005), and Engineering Research Centre of None-food Biomass Efficient Pyrolysis and Utilization Technology of Guangdong Higher Education Institutes (No. 2016GCZX009).

References

1. Y. Guo, N. Gao, Y. Bai, J. Zhao, and X. Zeng, Monolayered semiconducting GeAsSe and SnSbTe with ultrahigh hole mobility, *Front. Phys.* 13(4), 138117 (2018)
2. G. Zheng, L. Li, Z. Tian, X. Zhang, and L. Chen, Het-

erogeneous single-cluster catalysts (Mn_3, Fe_3, Co_3, and Mo_3) supported on nitrogen-doped graphene for robust electrochemical nitrogen reduction, *J. Energy Chem.* 54, 612 (2021)

3. Q. Li, L. He, C. Sun, and X. Zhang, Computational study of MoN_2 monolayer as electrochemical catalysts for nitrogen reduction, *J. Phys. Chem. C* 121(49), 27563 (2017)
4. G. Chen, Y. Yuan, H. Jiang, S. Ren, L. Ding, L. Ma, T. Wu, J. Lu, and H. Wang, Electrochemical reduction of nitrate to ammonia via direct eight-electron transfer using a copper–molecular solid catalyst, *Nat. Energy* 5(8), 605 (2020)
5. L. J. Arachchige, Y. Xu, Z. Dai, X. Zhang, F. Wang, and C. Sun, Theoretical investigation of single and double transition metals anchored on graphyne monolayer for nitrogen reduction reaction, *J. Phys. Chem. C* 124(28), 15295 (2020)
6. W. Gao, P. Wang, J. Guo, F. Chang, T. He, Q. Wang, G. Wu, and P. Chen, Barium hydride-mediated nitrogen transfer and hydrogenation for ammonia synthesis: A case study of cobalt, *ACS Catal.* 7(5), 3654 (2017)
7. P. Wang, F. Chang, W. Gao, J. Guo, G. Wu, T. He, and P. Chen, Breaking scaling relations to achieve low-temperature ammonia synthesis through LiH-mediated nitrogen transfer and hydrogenation, *Nat. Chem.* 9(1), 64 (2017)
8. C. Guo, J. Ran, A. Vasileff, and S. Qiao, Rational design of electrocatalysts and photo(electro)catalysts for nitrogen reduction to ammonia (NH_3) under ambient conditions, *Energy Environ. Sci.* 11(1), 45 (2018)
9. C. Lv, Y. Qian, C. Yan, Y. Ding, Y. Liu, G. Chen, and G. Yu, Defect engineering metal-free polymeric carbon nitride electrocatalyst for effective nitrogen fixation under ambient conditions, *Angew. Chem. Int. Ed.* 57(32), 10246 (2018)
10. G. Deng, T. Wang, A. A. Alshehri, K. A. Alzahrani, Y. Wang, H. Ye, Y. Luo, and X. Sun, Improving the electrocatalytic N_2 reduction activity of Pd nanoparticles through surface modification, *J. Mater. Chem. A* 7(38), 21674 (2019)
11. C. Liu, Q. Li, J. Zhang, Y. Jin, D. R. MacFarlane, and C. Sun, Conversion of dinitrogen to ammonia on Ru atoms supported on boron sheets: A DFT study, *J. Mater. Chem. A* 7(9), 4771 (2019)
12. Y. Hao, Y. Guo, L. Chen, M. Shu, X. Wang, T. Bu, W. Gao, N. Zhang, X. Su, X. Feng, J. Zhou, B. Wang, C. Hu, A. Yin, R. Si, Y. Zhang, and C. Yan, Promoting nitrogen electroreduction to ammonia with bismuth nanocrystals and potassium cations in water, *Nat. Catal.* 2(5), 448 (2019)
13. W. Wang, H. Zhang, S. Zhang, Y. Liu, G. Wang, C. Sun, and H. Zhao, Potassium-ion-assisted regeneration of active cyano groups in carbon nitride nanoribbons: Visible-light-driven photocatalytic nitrogen reduction, *Angew. Chem. Int. Ed.* 58(46), 16644 (2019)
14. G. P. Connor and P. L. Holland, Coordination chemistry insights into the role of alkali metal promoters in dinitrogen reduction, *Catal. Today* 286, 21 (2017)
15. D. Yao, C. Tang, L. Li, B. Xia, A. Vasileff, H. Jin, Y. Zhang, and S. Qiao, *In situ* fragmented bismuth nanoparticles for electrocatalytic nitrogen reduction, *Adv. Energy Mater.* 10(33), 2001289 (2020)
16. L. Kalarasse, B. Bennecer, and F. Kalarasse, Optical properties of the alkali antimonide semiconductors Cs_3Sb, Cs_2KSb, CsK_2Sb and K_3Sb, *J. Phys. Chem. Solids* 71(3), 314 (2010)
17. M. Kitano, S. Kanbara, Y. Inoue, N. Kuganathan, P. V. Sushko, T. Yokoyama, M. Hara, and H. Hosono, Electride support boosts nitrogen dissociation over ruthenium catalyst and shifts the bottleneck in ammonia synthesis, *Nat. Commun.* 6(1), 6731 (2015)
18. Z. Yi, Y. Qian, S. Jiang, Y. Li, N. Lin, and Y. Qian, Self-wrinkled graphene as a mechanical buffer: A rational design to boost the K-ion storage performance of Sb_2Se_3 nanoparticles, *Chem. Eng. J.* 379, 122352 (2020)
19. X. Huang, J. Deng, Y. Qi, D. Liu, Y. Wu, W. Gao, W. Zhong, F. Zhang, S. Bao, and M. Xu, A highly-effective nitrogen-doped porous carbon sponge electrode for advanced K–Se batteries, *Inorg. Chem. Front.* 7(5), 1182 (2020)
20. Y. Yi, Z. Sun, C. Li, Z. Tian, C. Lu, Y. Shao, J. Li, J. Sun, and Z. Liu, Designing 3D biomorphic nitrogen-doped $MoSe_2$/graphene composites toward high-performance potassium-ion capacitors, *Adv. Funct. Mater.* 30(4), 1903878 (2019)
21. I. Y. Jeon, M. Choi, H. J. Choi, S. M. Jung, M. J. Kim, J. M. Seo, S. Y. Bae, S. Yoo, G. Kim, H. Y. Jeong, N. Park, and J. B. Baek, Antimony-doped graphene nanoplatelets, *Nat. Commun.* 6(1), 7123 (2015)
22. A. Tang, M. Long, P. Liu, L. Tan, and Z. He, Morphologic control of Sb-rich Sb_2Se_3 to adjust its catalytic hydrogenation properties for p-nitrophenol, *RSC Adv.* 4(100), 57322 (2014)
23. L. Xu, L. Yang, and E. Ganz, Electrocatalytic reduction of N_2 using metal-doped borophene, *ACS Appl. Mater. Interfaces* 13(12), 14091 (2021)
24. S. Lv, C. Huang, G. Li, and L. Yang, Electrocatalytic mechanism of N_2 reduction reaction by single-atom catalyst rectangular TM-TCNQ monolayers, *ACS Appl. Mater. Interfaces* 13(25), 29641 (2021)
25. C. Huang, G. Li, L. M. Yang, and E. Ganz, Ammonia synthesis using single-atom catalysts based on two-dimensional organometallic metal phthalocyanine monolayers under ambient conditions, *ACS Appl. Mater. Interfaces* 13(1), 608 (2021)
26. K. Chu, Y. Liu, Y. Li, Y. Guo, and Y. Tian, Two-dimensional (2D)/2D interface engineering of a MoS_2/C_3N_4 heterostructure for promoted electrocatalytic nitrogen fixation, *ACS Appl. Mater. Interfaces* 12(6), 7081 (2020)
27. W. Fu, H. He, Z. Zhang, C. Wu, X. Wang, H. Wang, Q. Zeng, L. Sun, X. Wang, J. Zhou, Q. Fu, P. Yu, Z. Shen, C. Jin, B. I. Yakobson, and Z. Liu, Strong interfacial coupling of MoS_2/g-C_3N_4 van de Waals solids for highly active water reduction, *Nano Energy* 27, 44 (2016)

28. Y. Huang, T. Yang, L. Yang, R. Liu, G. Zhang, J. Jiang, Y. Luo, P. Lian, and S. Tang, Graphene-boron nitride hybrid supported single Mo atom electrocatalysts for efficient nitrogen reduction reaction, *J. Mater. Chem. A* 7(25), 15173 (2019)
29. Y. Tian, S. Hu, X. Sheng, Y. Duan, J. Jakowski, B. G. Sumpter, and J. Huang, Non-transition-metal catalytic system for N_2 reduction to NH_3: A density functional theory study of Al-doped graphene, *J. Phys. Chem. Lett.* 9(3), 570 (2018)
30. J. Jiang, Graphene versus MoS_2: A short review, *Front. Phys.* 10(3), 287 (2015)
31. B. Jiang, Y. Wang, C. Liao, Y. Chang, Y. Su, R. Jeng, and C. Chen, Improved blend film morphology and free carrier generation provide a high-performance ternary polymer solar cell, *ACS Appl. Mater. Interfaces* 13(1), 1076 (2021)
32. T. Xu, B. Ma, J. Liang, L. Yue, Q. Liu, T. Li, H. Zhao, Y. Luo, S. Lu, and X. Sun, recent progress in metal-free electrocatalysts toward ambient N_2 reduction reaction, *Wuli Huaxue Xuebao* 37, 2009043 (2021)
33. N. Zhao, J. Qin, L. Chu, L. Wang, D. Xu, X. Wang, H. Yang, J. Zhang, and X. Li, Heterogeneous interface of Se@Sb@C boosting potassium storage, *Nano Energy* 78, 105345 (2020)
34. Z. Yi, Y. Qian, J. Tian, K. Shen, N. Lin, and Y. Qian, Self-templating growth of Sb_2Se_3@microtube: A conversion-alloying-type anode material for enhanced K-ion batteries, *J. Mater. Chem. A* 7(19), 12283 (2019)
35. J. Chen, X. Xu, T. Li, K. Pandiselvi, and J. Wang, Toward high performance 2D/2D hybrid photocatalyst by electrostatic assembly of rationally modified carbon nitride on reduced graphene oxide, *Sci. Rep.* 6(1), 37318 (2016)
36. L. Xia, J. Yang, H. Wang, R. Zhao, H. Chen, W. Fang, A. M. Asiri, F. Xie, G. Cui, and X. Sun, Sulfur-doped graphene for efficient electrocatalytic N_2-to-NH_3 fixation, *Chem. Commun.* 55(23), 3371 (2019)
37. X. Yang and R. Zhang, High-capacity graphene-confined antimony nanoparticles as a promising anode material for potassium-ion batteries, *J. Alloys Compd.* 834, 155191 (2020)
38. K. S. Novoselov, D. V. Andreeva, W. Ren, and G. Shan, Graphene and other two-dimensional materials, *Front. Phys.* 14(1), 13301 (2019)
39. L. J. Arachchige, Y. Xu, Z. Dai, X. Zhang, F. Wang, and C. Sun, Double transition metal atoms anchored on graphdiyne as promising catalyst for electrochemical nitrogen reduction reaction, *J. Mater. Sci. Technol.* 77, 244 (2021)
40. Q. Li, S. Qiu, C. Liu, M. Liu, L. He, X. Zhang, and C. Sun, Computational design of single-molybdenum catalysts for the nitrogen reduction reaction, *J. Phys. Chem. C* 123(4), 2347 (2019)
41. Z. Cui, W. Du, C. Xiao, Q. Li, R. Sa, C. Sun, and Z. Ma, Enhancing hydrogen evolution of MoS_2 Basal planes by combining single-boron catalyst and compressive strain, *Front. Phys.* 15(6), 63502 (2020)
42. H. Zhang, C. Cui, and Z. Luo, MoS_2 supported Fe_2 clusters catalyzing nitrogen reduction reaction to produce ammonia, *J. Phys. Chem. C* 124(11), 6260 (2020)
43. Q. Li, C. Liu, S. Qiu, F. Zhou, L. He, X. Zhang, and C. Sun, Exploration of iron borides as electrochemical catalysts for the nitrogen reduction reaction, *J. Mater. Chem. A* 7(37), 21507 (2019)
44. D. Jiao, Y. Liu, Q. Cai, and J. Zhao, Coordination tunes the activity and selectivity of the nitrogen reduction reaction on single-atom iron catalysts: A computational study, *J. Mater. Chem. A* 9, 1240 (2021)
45. Y. Liu, Z. Tai, J. Zhang, W. Pang, Q. Zhang, H. Feng, K. Konstantinov, Z. Guo, and H. Liu, Boosting potassium-ion batteries by few-layered composite anodes prepared via solution-triggered one-step shear exfoliation, *Nat. Commun.* 9(1), 3645 (2018)
46. X. Hu, J. Zheng, and Z. Ren, Strong interlayer coupling in phosphorene/graphene van der Waals heterostructure: A first-principles investigation, *Front. Phys.* 13(2), 137302 (2018)
47. X. Guo, J. Gu, S. Lin, S. Zhang, Z. Chen, and S. Huang, Tackling the activity and selectivity challenges of electrocatalysts toward the nitrogen reduction reaction via atomically dispersed biatom catalysts, *J. Am. Chem. Soc.* 142(12), 5709 (2020)
48. L. Li, X. Wang, H. Guo, G. Yao, H. Yu, Z. Tian, B. Li, and L. Chen, Theoretical screening of single transition metal atoms embedded in MXene defects as superior electrocatalyst of nitrogen reduction reaction, *Small Methods* 3(11), 1900337 (2019)
49. Y. Huang, T. Yang, L. Yang, R. Liu, G. Zhang, J. Jiang, Y. Luo, P. Lian, and S. Tang, Graphene–boron nitride hybrid-supported single Mo atom electrocatalysts for efficient nitrogen reduction reaction, *J. Mater. Chem. A Mater. Energy Sustain.* 7(25), 15173 (2019)
50. Z. Feng, Y. Tang, W. Chen, D. Wei, Y. Ma, and X. Dai, O-doped graphdiyne as metal-free catalysts for nitrogen reduction reaction, *Mol. Catal.* 483, 110705 (2020)
51. X. Hu, Y. Sun, S. Guo, J. Sun, Y. Fu, S. Chen, S. Zhang, and J. Zhu, Identifying electrocatalytic activity and mechanism of $Ce_{1/3}NbO_3$ perovskite for nitrogen reduction to ammonia at ambient conditions, *Appl. Catal. B* 280, 119419 (2021)
52. T. M. Figg, P. L. Holland, and T. R. Cundari, Cooperativity between low-valent iron and potassium promoters in dinitrogen fixation, *Inorg. Chem.* 51(14), 7546 (2012)
53. Q. Zhang, B. Liu, L. Yu, Y. Bei, and B. Tang, Synergistic promotion of the electrochemical reduction of nitrogen to ammonia by phosphorus and potassium, *ChemCatChem* 12(1), 334 (2020)
54. Y. Liu, P. Deng, R. Wu, X. Zhang, C. Sun, and H. Li, Oxygen vacancies for promoting the electrochemical nitrogen reduction reaction, *J. Mater. Chem. A* 9(11), 6694 (2021)
55. M. A. Ahsan, T. He, K. Eid, A. M. Abdullah, M. L. Curry, A. Du, A. R. P. Santiago, L. Echegoyen, and J. C. Noveron, Tuning the intermolecular electron transfer of low-dimensional and metal-free BCN/C_{60} electrocatalysts via interfacial defects for efficient hydrogen and oxygen electrochemistry, *J. Am. Chem. Soc.* 143(2), 1203 (2021)

56. T. Wang, S. Qiu, Z. Dai, R. Hocking, and C. Sun, Exploration of TiO_2 as substrates for single metal catalysts: A DFT study, *Appl. Surf. Sci.* 533, 147362 (2020)
57. X. Chen, W. J. Ong, X. Zhao, P. Zhang, and N. Li, Insights into electrochemical nitrogen reduction reaction mechanisms: Combined effect of single transition-metal and boron atom, *J. Energy Chem.* 58, 577 (2021)
58. M. Yao, Z. Shi, P. Zhang, W. J. Ong, J. Jiang, W. Y. Ching, and N. Li, Density functional theory study of single metal atoms embedded into MBene for electrocatalytic conversion of N_2 to NH_3, *ACS Appl. Nano Mater.* 3(10), 9870 (2020)
59. M. Qu, G. Qin, J. Fan, A. Du, and Q. Sun, Theoretical insights into the performance of single and double transition metal atoms doped on N-graphenes for N_2 electroreduction, *Appl. Surf. Sci.* 537, 148012 (2021)
60. C. Liu, Q. Li, C. Wu, J. Zhang, Y. Jin, D. R. MacFarlane, and C. Sun, Single-boron catalysts for nitrogen reduction reaction, *J. Am. Chem. Soc.* 141(7), 2884 (2019)
61. X. Wang, S. Qiu, J. Feng, Y. Tong, F. Zhou, Q. Li, L. Song, S. Chen, K. H. Wu, P. Su, S. Ye, F. Hou, S. X. Dou, H. K. Liu, G. Q. Lu, C. Sun, J. Liu, and J. Liang, Confined Fe–Cu clusters as sub-nanometer reactors for efficiently regulating the electrochemical nitrogen reduction reaction, *Adv. Mater.* 32, 2004382 (2020)
62. L. Lin, Z. Shi, J. Huang, P. Wang, W. Y. C. He, and Z. Zhang, Molecular adsorption properties of CH_4 with noble metals doped onto oxygen vacancy defect of anatase TiO_2 (101) surface: First-principles calculations, *Appl. Surf. Sci.* 514, 145900 (2020)
63. J. Yu, C. He, C. Pu, L. Fu, D. Zhou, K. Xie, J. Huo, C. Zhao, and L. Yu, Prediction of stable BC_3N_2 monolayer from first-principles calculations: Stoichiometry, crystal structure, electronic and adsorption properties, *Chin. Chem. Lett.* (2021)
64. J. Wang, C. He, J. Huo, L. Fu, and C. Zhao, A theoretical evaluation of possible N_2 reduction mechanism on Mo_2B_2, *Adv. Theory Simul.* 4(5), 2100003 (2021)
65. M. Xiao, L. Zhang, B. Luo, M. Lyu, Z. Wang, H. Huang, S. Wang, A. Du, and L. Wang, Molten-salt-mediated synthesis of an atomic nickel co-catalyst on TiO_2 for improved photocatalytic H_2 evolution, *Angew. Chem. Int. Ed.* 132(18), 7297 (2020)